Available online at www.sciencedirect.com

SciVerse ScienceDirect

Procedia Chemistry 8 (2013) 239 – 247

Procedia Chemistry

Youth in Conservation of Cultural Heritage, YOCOCU 2012

Study of the early stages of Mn intrusion in corroded glass by means of combined SR FTIR/μXRF imaging and XANES spectroscopy.

Gert Nuyts[a]*, Simone Cagno[a], Kevin Hellemans[a], Giulia Veronesi[b], Marine Cotte[b], Koen Janssens[a]

[a]*Department of Chemistry, University of Antwerp, Groenenborgerlaan 171, 2020 Antwerp, Belgium*
[b]*ESRF, Rue Jules Horowitz, F-38043 Grenoble, France*

Abstract

Historical glass, especially medieval glass, can undergo weathering under the influence of time and environmental conditions. The aim of this investigation was to better understand the processes involved in this natural degradation process by studying artificially altered glass samples prepared for the use of evaluation of conservation methods. Non-durable glass sensors produced by the Fraunhöfer Institute (type M1.0) were used as a starting material for artificial alteration. These were immersed in acidic (pH = 0, 2, 4) and neutral solutions (1 h - 8 h). In a second stage the glass samples were immersed in a 0.5 M $MnCl_2$ solution (24 h, 48 h and 72 h), allowing intrusion of Mn from the solution into the gel layer. The samples were characterized at different stages with reflectance FTIR spectroscopy, μXRF mapping and μXANES. All measurements were carried out at ESRF, beamline ID21. Reflectance FTIR spectroscopy measurements were performed in the 800–4000 cm^{-1} range. Cluster analysis of the resulting maps evidenced the rapid growth of the gel layer in strong acidic conditions. The average spectra for each cluster feature show for the original glass a strong Si-O^- stretching band between 900 and 1000 cm^{-1}, whereas the gel layer could be identified by the increasing Si-O-Si bands around 1100 and 1250 cm^{-1}. μXRF maps were recorded at different stages of the experiment at energies around the Mn-K edge (6.539 keV) and with a step size of 2 by 2 μm. These confirm the leaching of K^+ and Ca^{+2} from the glass and the intrusion of Mn from the solution. Mn was found throughout the entire gel layer, but with a concentration gradient peaking at the surface. XANES point measurements were recorded at various points where Mn was present. No spatial variation was found, but linear combination fitting of the spectra with various Mn reference compounds indicated that $Mn^{2+}Mn^{3+}{}_2O_4$ is the main Mn compound in the gel layer, as was hypothesised by Watkinson et al. The standard corroded glass samples studied here can be used for the evaluation of conservation treatments in follow-up experiments.

Selection and peer-review under responsibility of the IA-CS (Italian Association of Conservation Scientists) and University of Antwerp

Keywords: weathering; Mn intrusion; Mn_3O_4

* Corresponding author. Tel.:+3232653326; fax: +3232653233.
E-mail address: Gert.Nuyts@ua.ac.be

1876-6196 © 2013 The Authors. Published by Elsevier B.V.
Selection and peer-review under responsibility of the IA-CS (Italian Association of Conservation Scientists) and University of Antwerp
doi:10.1016/j.proche.2013.03.030

1. Introduction

Since the alteration of silicate glass is discussed in this paper, a brief summary of the different steps of the weathering of historical glass is presented hereafter. A more detailed description can be found in literature [1] .
Generally the weathering of silicate glass is induced by the presence of water [2]. As a first step, molecular water penetrates into the glass via molecular diffusion and/or reversible hydrolysis/condensation reactions. As a result the silica network will undergo structural transformations [3, 4]. In case of glass buried in wet soil, ppm amounts of molecular water will diffuse into the glass, causing the breaking and forming of silicon-oxygen bonds [5, 6]:

$$\equiv Si–O–Si\equiv + H_2O_{(aq.)} \rightarrow 2\ \equiv Si–O–H$$
$$2\ \equiv Si–O–H \rightarrow \equiv Si–O–Si\equiv + H_2O_{(glass)}$$

In a second step, an ion exchange process will take place between protons from the environment and cations present within the glass network [7, 8]. This will only take place at low pH values and will result in the leaching out of most mobile cations (i.e., monovalent Na^+ and K^+). During this process the density of the leached layer will decrease since heavier metal cations are being replaced by lighter protons. On the glass surface, weathering products (i.e., sulfates and chlorides of Mg, Ca, etc.) can be formed [9-12].

$$\equiv Si–O^- M^+_{(glass)} + H^+_{(aq.)} \rightarrow \equiv Si–O^- H^+_{(glass)} + M^+_{(aq.)}$$

Finally, the local pH can rise if the water is not (regularly) replenished due to the ongoing proton exchange. When pH values typically exceed 9, the silica network will be attacked by hydroxyl ions [13] leading to further degradation.

$$\equiv Si–O–Si\equiv + {}^-OH_{(aq.)} \rightarrow \equiv Si–OH + {}^-O–Si\equiv$$
$$\equiv Si–O^- + H_2O \rightarrow \equiv Si–O–H + {}^-OH_{(aq.)}$$

The three aforementioned steps will cause the formation of a leached layer, being nothing more than a cation depleted silica network characterized by a lower density compared to the original healthy glass as well as a changed expansion coefficient. If none of the mentioned conditions change, this layer will gradually increase in thickness and the change of expansion coefficient will lead to stress between the leached layer and the original glass, which can eventually result in a part of the leached layer cracking off. This will expose a fresh surface of the original glass.
As described elsewhere in more detail [1], when a manganese source is available, manganese rich bodies can be formed inside the leached layer. Historical glass often contains a small amount of manganese (typically 0.5-1 wt %) with Mn(II) being the predominant species and only a small fraction is found having a higher oxidation state. Manganese can be present in the glass as an impurity of the raw materials (wood ash, etc.) or can have been added deliberately as pyrolusite (MnO_2), a decolorizing agent, in order to oxidize the strongly coloring Fe(II) ions to less coloring Fe(III) [14]. Alternatively, manganese can also have been introduced into the glass from the soil in which the glass is buried as dissolved Mn(II). In both cases a diffusion controlled Mn flux can result in the presence of dissolved Mn(II) in the lower density lamellae [1]. Previous experiments have indicated the presence of MnO_2 in the Mn rich bodies and a hypothesis for their formation was proposed [1]: in the presence of water and oxygen, Mn(II) and/or Mn(III) ions can be oxidized to higher oxidation states giving rise to, for example, insoluble MnO_2 that then can precipitate in the above-mentioned lower density voids, a process favoured in alkaline conditions

$$Mn^{2+} + ½O_2 + 2OH^- \leftrightarrow MnO_2\downarrow + H_2O$$

The aim of this investigation was to contribute to the understanding of processes involved in the natural degradation of historical glass by simulating accelerated weathering under controlled conditions, and, as a consequence, to create artificially altered glass samples for the use of evaluation of conservation methods. As a starting material, Fraunhöfer type M1.0 sensor glass (54.2 wt% SiO_2, 28.8 wt% K_2O, 17.0 wt% CaO) [15]was

used, which contains no manganese and has a low durability. In order to facilitate and accelerate the weathering process, a two step treatment was chosen. The first step was the creation of a leached/hydrated layer on the contact surface between the glass and the treatment solution. In order to assure the creation of a leached layer in an acceptable time period an HCl solution was chosen for this purpose. Since no manganese is present in the M1.0 glass, an external manganese source was needed. In a second step, glass samples were immersed in a 0.5 M $MnCl_2$ solution to create Mn intrusions. In both cases glass fragments were immersed in an excess solution. Characterization of the glass samples was performed with SR based microscopic Fourier-transform infra-red spectroscopy (μFTIR), microscopic X-ray fluorescence analysis (μXRF) mapping and microscopic X-ray absorption near edge spectroscopy (μXANES); the latter method allows to perform speciation on low concentration levels of Mn in glass without an elaborate sample preparation. The aim is to record μFTIR maps of the glass fragments by exploiting the high brilliance of SR radiation; this allows to record maps in a reasonable time span (3 h). All measurements were carried out at beam line ID21, ESRF.
Since in-depth information on the leaching process and Mn intrusion is sought-after, cross sections of the treated glass fragments are needed. In order to enable physical cutting and polishing each glass fragment was embedded in acrylic resin after treatment. All analyzes were performed on the obtained cross sections.

2. Experimental

XAS/XRF data collection

XANES spectra at the Mn-K edge were collected at the European Synchrotron Radiation Facility (ESRF, Grenoble, France), on beam line ID21 with an undulator insertion device. The storage ring operating conditions were 6 GeV electron energy with 200 mA electron current in 7/8 multibunch mode. For these experiments a Si (111) double-crystal monochromator was used, having an energy resolution of ca 10^{-4}($\Delta E/E$). Two mirrors were used to remove the high-energy harmonics from the incident X-ray beam. A Mn reference foil was used to provide the energy calibration for all the XANES spectra (first inflection point of the Mn K-edge edge set at 6539 eV [16]). Most Mn reference compounds were measured in fluorescence mode as well as in transmission mode. The mineral reference compounds were ground using a mortar. In order to avoid contributions of possible heterogeneities, measurements were performed with an unfocused beam using a 100 μm pinhole. XANES spectra were recorded with the sample positioned at 45º with respect to the incoming beam. The fluorescence yield was recorded as a function of the X-ray energy using a photodiode at an angle of 45º with respect to the sample. XANES spectra were collected from ~20 eV below to ~90 eV above the Mn K edge (6520 eV – 6629.5 eV), with 0.3 eV steps for the entire region. 100 ms integration time was used for each energy, resulting in ~ 45 s measuring time for one XANES spectrum. Five repeats were recorded for each Mn model compound in order to acquire noise free spectra. μXRF mapping and μXANES measurements of the glass samples were performed with a focused beam, using Fresnel zone plate focusing optics. The resulting beam size of 0.3 by 0.8 micron beam size allowed us to examine the intruded Mn. In order to prevent beam damage during the XANES measurements (auto-oxidation) the beam was slightly defocused resulting in a spot size of 5 x 5 μm^2. During the μXRF mapping, a 2 μm step size in both dimensions and a measuring time of 500 ms/pt was applied in order to prevent auto-oxidation**.** The thickness of the embedded samples prevented transmission measurements and only the SDD was used to monitor the fluorescence yield as a function of the energy of the X-ray beam. Several repeats with a maximum of five were recorded for each measured point to acquire noise free spectra. For all the XANES spectra, the normalization was performed by means of ATHENA, a software package widely used for XAFS data analysis. An edge-step normalization was performed by a linear pre-edge subtraction and by regression of a (in general) quadratic polynomial beyond the edge [17]. If the silicon drift detector was used for the collection of XANES spectra, the recorded XRF spectra were evaluated using the PyMCA software package. The fitted Mn intensity can then be plotted as a function of the excitation energy resulting in a (fluorescence mode) XANES spectrum.

FTIR spectroscopy

Synchrotron radiation was used as IR source for the different sample measurements. All FTIR measurements were performed at the IR end station of the ID21 beam line at ESRF (Grenoble, France), operating under the same conditions as described in XAS/XRF data collection. Synchrotron radiation has the advantage in comparison with classical sources to result in higher beam intensity. The peak-to-peak (ptp) value of SR radiation with an electron current of 200 mA is 11.1, while the internal Globular source (lab source) only has a ptp value of 0.63. Both values were obtained at the beam line by reflection on a gold mirror. Although SR has a lower brightness then infrared lasers, it provides a broad spectral emission making FTIR possible. Samples were measured with a Thermo Nicolet Continuum Microscope in specular reflection mode. An aperture of 15x15 µm² was used to obtain FTIR maps, conditions in which a good balance between resolution and signal to noise ratio was obtained. Every point on a map was the average of 50 scans. As the required information about the glass corrosion process could be deduced from the reflection spectra (800 cm^{-1} – 4000 cm^{-1}), the spectra presented here were not converted to absorption spectra in order to eliminate conversion errors. On the vector normalised maps, hierarchical cluster analysis was performed (using Ward's clustering strategy) with MATLAB in order to determine possible phases in the glass. Background spectra were collected by means of a gold mirror. The advantages of SR µFTIR in cultural heritage are described in greater detail in literature [18].

3. Results and discussion

SR µFTIR mapping

When hierarchical cluster analysis was performed on the treated glass samples, three clusters were observed. The average spectra of each cluster are given in Figure 1, confirming our assumptions about the designation of the clusters. The embedding resin of the glass sample (red line) shows a characteristic carboxylic band around 1700 cm^{-1} while the original glass (blue line) shows a strong $Si\text{-}O^-$ stretching band between 900 and 1000 cm^{-1}; the leached glass layer on the other hand can be identified by increasing Si-O-Si bands around 1100 and 1250 cm^{-1}.

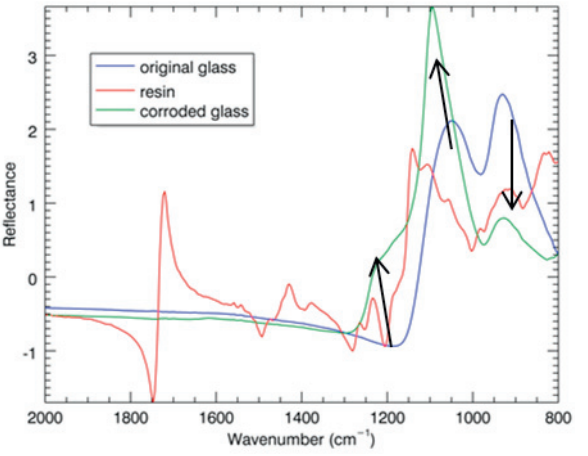

Figure 1: Figure showing the average reflection IR spectra of the different clusters. The black arrows show the changes in the IR spectra during glass alteration.

It is found in literature that during leaching the ($Si\text{-}O^-$):(Si-O-Si) ratio lowers, which can be observed in the reflection spectra as a lowering of the $Si\text{-}O^-$ stretch and an increase of the Si-O-Si antisymmetric stretch as is shown by the black arrows in Figure 1 [19, 20]. This cluster analysis can thus be used to monitor the weathering and degradation of the silica network. In Figure 2 a treatment series is shown in which a glass fragment has been placed in a 1 M HCl solution during 0h, 3h and 6h (Figure 2 a, b and c respectively); the same colours as in Figure 1 were used to represent the clusters. Figure 2 represents not only morphological information, but also chemical fingerprinting of the different areas. As could be expected, from this figure it becomes clear that the leached layer grows rapidly in strong acidic conditions, and reaches a depth of 40-50 µm after 6 h. Since the resolution of these maps is 15x15 µm², this depth has to be interpreted with care and will be evaluated with a better resolution during the discussion of the µXRF results.

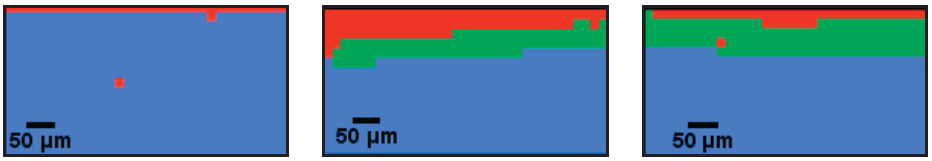

Figure 2: Results of hierarchical cluster analysis on the µFTIR maps after (a) 0 h, (b) 3 h and (c) 6 h in 1M HCl solution. (blue = original glass, green = corroded glass, red = resin).

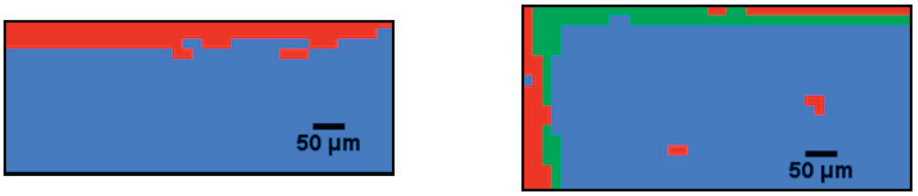

Figure 3: Results of hierarchical cluster analysis on the µFTIR maps after (a) 4 h in pH 4 solution, (b) 6 h in a pH 7 solution. (blue = original glass, green = corroded glass, red = resin).

In order to assess the validity of our results, it is of great importance to investigate whether or not similar behaviour occurs under less acidic conditions, as in realistic burial conditions, archaeological glass samples usually are not subject to such harsh conditions. Therefore similar leaching experiments were also performed on different glass fragments. For instance using more diluted HCl solutions in the leaching step, resulting in higher pH values. Results show that corrosion already sets in after 4 h in a solution at pH 4 (Figure 3a), comparable to acid rain. As can be expected, no significant deterioration was observed during another leaching experiment at neutral pH within the timeframe of the experiment (Figure 3b). Although these findings confirm what is already known in literature, it is clear that SR µFTIR can be used as a monitoring tool for unambiguous monitoring of alterations in the silica network during the leaching of earth alkali and alkali metals from the glass network.

SR µXRF mapping

Evaluation of the leaching process can be monitored using SR µFTIR allowing characterization of the structure of the silica network, but additional information is still required to characterize all the processes involved in the artificial weathering. SR µXRF allows the monitoring of the actual leaching of the present cations and the possible intrusion of Mn after immersion in a 0.5 M $MnCl_2$ solution. In Figure 4 the elemental distribution maps of Si, Ca and Mn of a treatment series are shown. This series consist of an immersion in 1 M HCl solution for 2 h, 4 h and 6 h and consequently 24h in 0.5 M $MnCl_2$ solution. In the Ca elemental distribution maps it can be observed that Ca is leached out of the glass fragment relatively rapid and leaches homogeneously (in the absence of cracks). The same can be observed in the elemental distribution maps of Si; here an apparent enrichment of Si is observed in the leached layer. This can be explained by the leaching out of the alkali and alkaline earth metals, causing the relative amount of Si in that area to increase. In addition to the leaching of cations, SR µXRF can also be used to monitor the intrusion of Mn inside the leached layer, as can be seen in the elemental distribution maps of Mn in Figure 4. Since it is quite difficult to ascertain whether or not Mn is present inside the leached layer or as a deposited layer on the glass surface, it can be useful to extract line profiles from the acquired data set as is shown in Figure 5. The elemental distribution maps (figure 4) could be used to determine the leaching depth (figure 5) of each cation since it is possible to look at the intensity profile of elements alongside a line perpendicular to the surface (figure 5e). The experiment pointed out that the leaching depth is +/- equal for K and Ca, but that K is leached out completely while Ca partially remains behind in the leached layer, in good agreement with the difference in mobility between K^+ and Ca^{2+}. The thickness of the leached layer reaches a maximum of +/- 58 µm after 6 h in 1M HCl (red line figure 5f). Furthermore the line profiles demonstrate that Mn has indeed penetrated the leached layer, since Mn is found together with Si. A concentration gradient is found, with the highest amount of precipitated Mn on the original surface. µXANES could then be used to determine the speciation of Mn on different locations inside and on top of the leached layer.

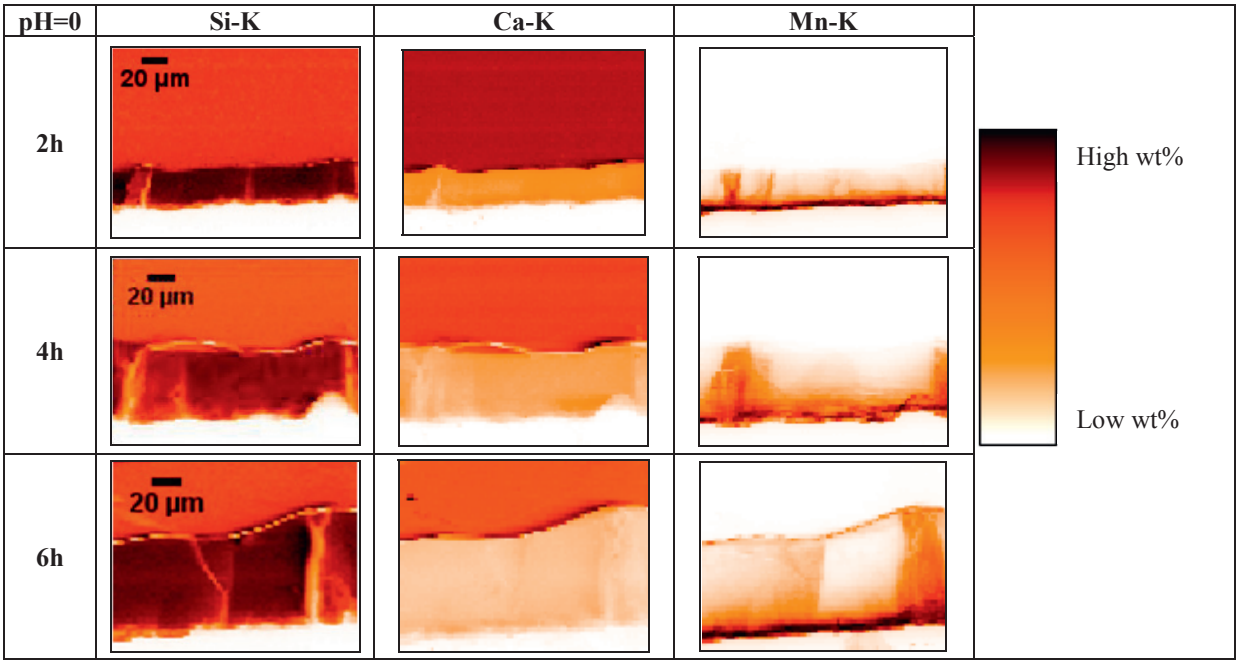

Figure 4: The net elemental intensities of different elements are used to create elemental X-ray maps. Si, K, Ca and Mn maps of a treatment with HCl (pH 0) and consecutive treatment with 0.5 M $MnCl_2$ (24 h).

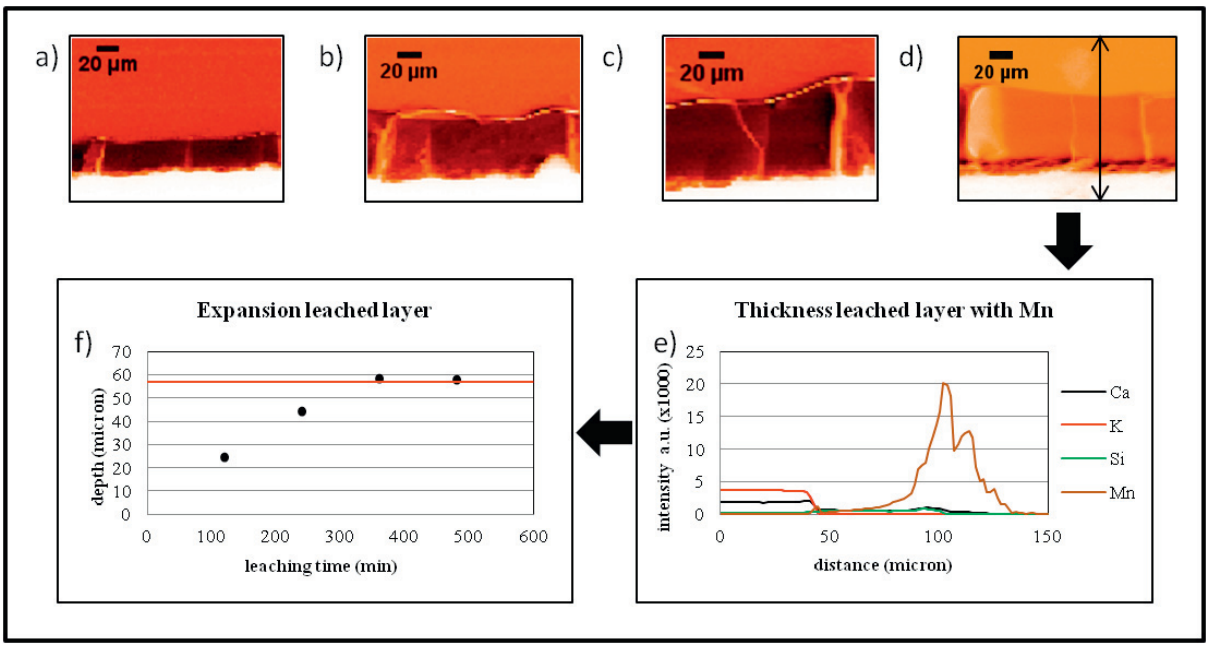

Figure 5: Determination of the leaching depth in 1M HCl-solution in function of the treatment time ((a) 2h, (b) 4h, (c) 6h and (d) 8h), (e) shows the intensity (a.u.) of K-K, Ca-K, Mn-K and Si-K line in function of the depth, the thickness of the Si-enriched layer is used as a reference for the leaching depth in (f).

µXANES

It is clear that Mn has effectively intruded into the glass, and more precisely into the leached layer. Since all glass fragments were immersed into a $MnCl_2$ solution it is highly probably that the manganese entered the glass as Mn^{2+} ions. In historically weathered glass Mn is often found in a highly oxidized state (e.g. MnO_2) resulting in the existence of conservation treatments that are based on reduction of highly oxidized Mn to the more mobile Mn^{2+}. For this reason, some glass fragments were also treated with a 1% v/v H_2O_2 solution after immersion in $MnCl_2$ in an attempt to oxidize the Mn^{2+} that previously entered the glass. The glass fragments containing Mn were characterized with Mn-K edge XANES after immersion in $MnCl_2$ and after immersion in hydrogen peroxide, µXRF maps could be used to locate Mn inside the leached layer. All measured spectra were processed as described in the experimental section and fitted using a linear combination of the following Mn reference compounds: K_2MnO_4, $KMnO_4$, $MnCl_2$, $MnSO_4.H_2O$, MnO, Mn_2O_3, MnO_2, Mn(II)acetate, Mn(III)acetate, commercial Mn brown pigment (hausmannite, Mn_3O_4), commercial Mn grey pigment (mixture MnO/MnO_2), and pyroxmangite ($Mn^{2+}_{0.8}Fe^{2+}_{0.2}SiO_3$). As a result of this LCF the weight percentages of all Mn compounds can be determined in relation to the total amount of all the Mn compounds present. The most dominant species of Mn in every sample before and after treatment with peroxide proved to be $Mn^{2+}Mn^{3+}{}_2O_4$ (reference compound spectrum in all the LCF was that of the mineral hausmannite) as was hypothesised by Watkinson, et al. [21].

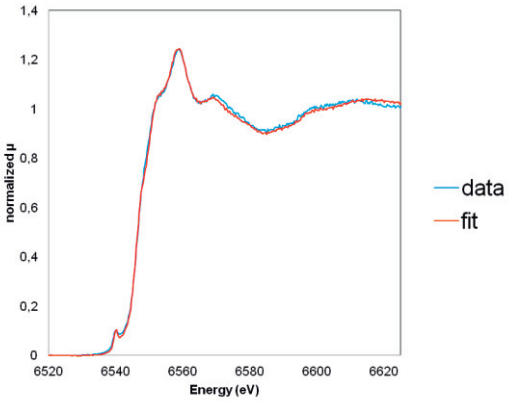

Figure 6: The unknown XANES spectra are expressed as a linear combination of the reference compound spectra. The fit of 2 h HCl (pH 0) and consecutive 24 h 0.5 M $MnCl_2$ treatment is given as example (75% Hausmannite, 25% manganese (1 wt%) in glass network in reference glass or $MnCl_2$).

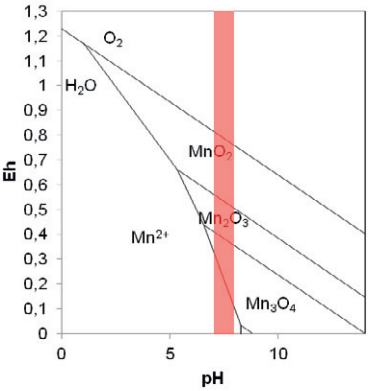

Figure 7: Figure shows the Pourbaix diagram of the Mn-O-H system (aq.) at 1 bar and assuming a dissolved species activity of 0.01. The pH area of the treatment with 0.5 M $MnCl_2$ is shown by the red bar.

This XAS analysis does not allow any assumptions to be made regarding the cristallinity of the Mn_3O_4. In Figure 6, a linear combination fit of a XANES point spectrum on a glass fragment that has been immersed in 1 M HCl for 2 h and a consecutively 24 h in a 0.5 M $MnCl_2$ solution is shown as an example. The point spectrum was taken at approximately 30 µm below the original surface at an induced crack. The result of this fit indicated that ca 75% of the Mn is present as Mn_3O_4 and 25% as $MnCl_2$ or Mn in (1wt %) reference glass.(LCF including $MnCl_2$ or Mn in reference glass give an equal fit). No significant spatial variation was found on the analyzed glass fragments nor any variation with treatment time. The Pourbaix diagram (Figure 7) of a Mn-O-H system [22-24] shows that in a neutral/slightly acidic environment MnO_2 is expected to be the most stable compound instead of Mn_3O_4; however the absence of MnO_2 and the presence of Mn_3O_4 in the studied samples indicates that the formation of the latter is most likely kinetically favoured and that possible further oxidation (e.g., to MnO_2) even in the presence of hydrogen peroxide can occur, but only in a longer time. Secondly these findings prove that Mn^{2+} can be oxidized solely by the presence of dissolved oxygen, since also glass fragments that were not treated with hydrogen peroxide contain Mn_3O_4.

4. Conclusions

This experiment was a first attempt to create artificially weathered glass in order to use it in a later stage as reference weathered glass during the evaluation of treatment methods for archaeological glass fragments. The intrusion of Mn from the $MnCl_2$-solution into standard non-durable and pre-leached glass was demonstrated. Naturally weathered historical glass often shows MnO_2 inclusions, giving it a black colour. Instead of MnO_2 (pyrolusite), however it was observed that Mn_2O_3 precipitated at neutral pH ($MnCl_2$ solution); thermodynamical analysis of the Mn-O-H system (figure 7) points out that in the conditions employed, MnO_2 is expected to be more stable than Mn_3O_4. This means that the formation of Mn_3O_4 is kinetically favoured over the formation of MnO_2 and further oxidation of Mn_3O_4, being a solid state reaction, is most likely to be very slow. In order to avoid this problem for future experiments, glass fragments will be submerged in a $MnCl_2$ solution buffered at pH +/- 4; in this pH region MnO_2 still is the most stable Mn compound while Mn_3O_4 should not be formed.
The use of SR FTIR allowed us to study the formation of a leached layer on glass under acidic conditions, which would not have been possible when using the traditional macro FTIR technique. Moreover, the high flux of the IR beam proved vital to obtain spectra in a fast and reliable manner, as the experiment might have taken weeks to complete with globarIR sources. We can also conclude from the artificial corrosion experiments at pH 4 that leaching of glass can occur in even slightly acidic environments, giving rise to the need of treatments for this effect.

Acknowledgements

This research was supported by the Interuniversity Attraction Poles Programme - Belgian Science Policy (IUAP VI/16). The text also presents results of GOA XANES “meets ELNES” (Research Fund University of Antwerp, Belgium) and from FWO (Brussels, Belgium) projects no. G.0704.08 and G.01769.09. We gratefully acknowledge ESRF for granting beamtime (experiment EC873).

References

[1] Schalm, O., et al., *MANGANESE STAINING OF ARCHAEOLOGICAL GLASS: THE CHARACTERIZATION OF Mn-RICH INCLUSIONS IN LEACHED LAYERS AND A HYPOTHESIS OF ITS FORMATION.* Archaeometry, 2011. **53**: p. 103-122.

[2] Conradt, R., *Chemical durability of oxide glasses in aqueous solutions: A review.* Journal of the American Ceramic Society, 2008. **91**(3): p. 728-735.

[3] Bunker, B.C., *MOLECULAR MECHANISMS FOR CORROSION OF SILICA AND SILICATE-GLASSES.* Journal of Non-Crystalline Solids, 1994. **179**: p. 300-308.

[4] Doremus, R.H., *Diffusion of water and oxygen in quartz: reaction-diffusion model.* Earth and Planetary Science Letters, 1998. **163**(1-4): p. 43-51.

[5] Sterpenich, J. and G. Libourel, *Water diffusion in silicate glasses under natural weathering conditions: evidence from buried medieval stained glasses.* Journal of Non-Crystalline Solids, 2006. **352**(50-51): p. 5446-5451.

[6] Zotov, N., et al., *The effect of water on the structure of silicate glasses - A neutron diffraction study.* Journal of Non-Crystalline Solids, 1996. **202**(1-2): p. 153-163.

[7] Melcher, M. and M. Schreiner, *Statistical evaluation of potash-lime-silica glass weathering.* Analytical and Bioanalytical Chemistry, 2004. **379**(4): p. 628-639.

[8] Scholze, H., *CHEMICAL DURABILITY OF GLASSES.* Journal of Non-Crystalline Solids, 1982. **52**(1-3): p. 91-103.

[9] Domenech-Carbo, M.T., et al., *A study on corrosion processes of archaeological glass from the Valencian Region (Spain) and its consolidation treatment.* Microchimica Acta, 2006. **154**(1-2): p. 123-142.

[10] Schreiner, M., et al., *Characterisation of surface layers formed under natural environmental conditions on medieval stained glass and ancient copper alloys using SEM, SIMS and atomic force microscopy.* Journal of Analytical Atomic Spectrometry, 1999. **14**(3): p. 395-403.

[11] Melcher, M. and M. Schreiner, *Leaching studies on naturally weathered potash-lime-silica glasses.* Journal of Non-Crystalline Solids, 2006. **352**(5): p. 368-379.

[12] Woisetschlager, G., et al., *Weathering phenomena on naturally weathered potash-lime-silica-glass with medieval composition studied by secondary electron microscopy and energy dispersive microanalysis.* Mikrochimica Acta, 2000. **135**(3-4): p. 121-130.

[13] Paul, A., *CHEMICAL DURABILITY OF GLASSES - THERMODYNAMIC APPROACH.* Journal of Materials Science, 1977. **12**(11): p. 2246-2268.

[14] Sayre, E.V., *The intentional use of antimony and manganese in acient glasses.* Advances in glass technology, 1963. **part 2**: p. 263-282.

[15] Fuchs, D.R., H. Romich, and H. Schmidt, *GLASS-SENSORS - ASSESSMENT OF COMPLEX CORROSIVE STRESSES IN CONSERVATION RESEARCH*. Materials Issues in Art and Archaeology Ii, ed. P.B. Vandiver, J. Druzik, and G.S. Wheeler. Vol. 185. 1991, Pittsburgh: Materials Research Soc. 239-251.

[16] McMaster, W.H., et al., eds. *Compilation of X-ray cross sections* 1969.

[17] Ravel, B. and M. Newville, *ATHENA, ARTEMIS, HEPHAESTUS: data analysis for X-ray absorption spectroscopy using IFEFFIT.* Journal of Synchrotron Radiation, 2005. **12**: p. 537-541.

[18] Cotte, M., et al., *Recent applications and current trends in Cultural Heritage Science using synchrotron-based Fourier transform infrared micro-spectroscopy.* Comptes Rendus Physique, 2009. **10**(7): p. 590-600.

[19] Lynch, M.E., D.C. Folz, and D.E. Clark, *Use of FTIR reflectance spectroscopy to monitor corrosion mechanisms on glass surfaces.* Journal of Non-Crystalline Solids, 2007. **353**(27): p. 2667-2674.

[20] El-Batal, F.H., et al., *FTIR Spectral Analysis of Corrosion Mechanisms in Soda Lime Silica Glasses Doped with Transition Metal Oxides.* Silicon, 2010. **2**(1): p. 41-47.

[21] Watkinson, D., L. Weber, and K. Anheuser, *Staining of archaeological glass from manganese-rich environments.* Archaeometry, 2005. **47**: p. 69-82.

[22] Patnaik, P., *Handbook of inorganic chemicals*. 2003: McGraw-Hill.

[23] Wagman, D.D., et al., *Selected values of chemical thermodynamic properties. Tables for the first thirty-four elements in the standard order of arrangement.* National Bureau of Standards (U.S.), technical note 1968: p. 270-273.

[24] Robie, R.A., B.S. Hemingway, and J.R. Fisher, *Thermodynamic properties of minerals and related substances at 298.15 K and 1 bar (10/sup 5/pascals) pressure and at higher temperatures.* U.S. Geology Survey Bulletin, technical note, 1978.